The value of high-frequency, high-precision methane isotopologue measurements for source and sink estimation

Citation: Rigby, M., A. J. Manning, and R. G. Prinn. "The Value of High-Frequency, High-Precision Methane Isotopologue Measurements for Source and Sink Estimation." Journal of Geophysical Research: Atmospheres 117, no. D12 (June 27, 2012): D12312.

As Published: http://dx.doi.org/10.1029/2011jd017384

Publisher: American Geophysical Union

Persistent URL: http://hdl.handle.net/1721.1/86178

Version: Final published version: final published article, as it appeared in a journal, conference proceedings, or other formally published context

The value of high-frequency, high-precision methane isotopologue measurements for source and sink estimation

M. Rigby,[1,2] A. J. Manning,[3] and R. G. Prinn[2]

Received 30 December 2011; revised 14 May 2012; accepted 19 May 2012; published 30 June 2012.

[1] We present an observing system simulation experiment examining the potential benefits of new methane isotopologues measurements for global- and national-scale source and sink inversions. New measurements are expected in the coming years, using quantum cascade laser spectroscopy with sample preconcentration, that will allow observations of $\delta^{13}C$ - CH_4 and δD - CH_4 at approximately hourly intervals and higher precision than previously possible. Using model-generated 'pseudo-data', we predict the variability that these new systems should encounter in the atmosphere, and estimate the additional uncertainty reduction that should result from their use in source and sink inversions. We find that much of the δ-value variability from seasonal to daily timescales should be resolvable at the target precision of the new observations. For global source estimation, we find additional uncertainty reductions of between 3–9 Tg/year for four major source categories (microbial, biomass burning, landfill and fossil fuel), compared to mole fraction-only inversions, if the higher end of the anticipated isotopologue-measurement precisions can be achieved. On national scales, we obtain average uncertainty reductions of ~10% of the source strength for countries close to high-frequency monitoring sites, although the degree of uncertainty reduction on such small scales varies significantly (from close to 0% to almost 50%) for different sources and countries.

Citation: Rigby, M., A. J. Manning, and R. G. Prinn (2012), The value of high-frequency, high-precision methane isotopologue measurements for source and sink estimation, *J. Geophys. Res.*, *117*, D12312, doi:10.1029/2011JD017384.

1. Introduction

[2] Observations of atmospheric methane (CH_4) mole fractions, along with chemical transport models (CTMs), have provided valuable information on the sources and sinks of this potent greenhouse gas [e.g. *Bousquet et al.*, 2006; *Chen and Prinn*, 2006; *Rigby et al.*, 2008; *Frankenberg et al.*, 2008; *Bergamaschi et al.*, 2009]. However, much uncertainty remains about the partitioning of CH_4 sources and the drivers of its inter-annual variability. Measurements of the isotopologues of CH_4 may provide additional information, since different sources emit with differing isotopic signatures [e.g., *Snover et al.*, 2000; *Whiticar and Schaefer*, 2007]. Furthermore, isotopic fractionation occurs due to the varying reaction rates of the isotopologues with methane sinks, potentially allowing us to further constrain methane destruction rates [e.g., *Saueressig et al.*, 2001].

[3] Previous measurements of CH_4, and its two most abundant isotopologues, $^{13}CH_4$ and CH_3D, have used tunable diode laser spectrometers or gas chromatography with mass spectrometry. These observations have been made during monthly to yearly campaigns [*Lowe et al.*, 1999; *Bergamaschi et al.*, 2000] or over many years at ~monthly resolution at a small number of sites [*Lowe et al.*, 1997; *Miller et al.*, 2002; *Tyler et al.*, 2007; *Dlugokencky et al.*, 2009]. Studies have shown that the seasonal cycles and trends in these observations can be well represented by atmospheric CTMs [*Allan et al.*, 2001], and that comparisons of CTM simulations with isotopic data may help to identify emissions variations over multidecadal timescales [*Hein et al.*, 1997; *Mikaloff-Fletcher*, 2004a, 2004b; *Monteil et al.*, 2011].

[4] Recent developments in infrared laser absorption spectroscopy with continuous wave quantum cascade lasers, along with gas preconcentration techniques, bring forward the possibility of measuring these isotopologues at higher frequency (~hourly intervals) and precision than has previously been possible [e.g., *Nelson et al.*, 2008; *Tuzson et al.*, 2008; *Zahniser et al.*, 2009; *Potter*, 2011].

[5] In light of these developments, this paper aims to critically evaluate the potential benefits of a global network of high-precision CH_4 isotopologue observations for inverse modeling. The investigation will be framed around two existing global networks: the Advanced Global Atmospheric Gases Experiment (AGAGE) [*Prinn et al.*, 2000] and the National Oceanic and Atmospheric Administration (NOAA) Carbon Cycle Greenhouse Gases (CCGG) cooperative sampling network [*Dlugokencky et al.*, 2009]. AGAGE is chosen to reflect a possible setup of a new in situ CH_4 isotopologue

[1]Center for Global Change Science, Massachusetts Institute of Technology, Cambridge, Massachusetts, USA.
[2]School of Chemistry, University of Bristol, Bristol, UK.
[3]Atmospheric Dispersion Group, UK Met Office, Exeter, UK.

Corresponding author: M. Rigby, School of Chemistry, University of Bristol, Cantock's Close, Bristol BS8 1TS, UK. (matt.rigby@bristol.ac.uk)

0148-0227/12/2011JD017384

network, which could make measurements at high-frequency, but at a limited number of sites. In contrast, the NOAA CCGG network represents an alternative setup in which flask samples are collected and measured at a central laboratory at lower frequency (∼ weekly), but at a larger number of locations.

[6] So called 'top-down' estimates of CH_4 emissions and sinks have been made in many studies using 'Bayesian' inverse methods [e.g., *Bousquet et al.*, 2006; *Chen and Prinn*, 2006; *Rigby et al.*, 2008; *Bergamaschi et al.*, 2009; *Frankenberg et al.*, 2008]. In these inversions, some prior information is assumed to exist about the likely sources and sinks of atmospheric CH_4 and their uncertainties. The initial uncertainty placed on these estimates is reduced through the incorporation of atmospheric observations, which are related to emissions using CTM-derived 'sensitivity' functions (usually assuming perfect transport and chemistry). The amount of uncertainty reduction depends on the number of observations, their uncertainty and the sensitivity of the observations to changes in emissions or sinks. Further information on Bayesian and other inverse methods can be found in many sources, for example, *Tarantola* [2005].

[7] From this Bayesian perspective, we will primarily focus on two questions: (1) By how much might we expect the uncertainty in top-down estimates of the major global CH_4 sources to be decreased, if observations of the major CH_4 isotopologues were made by networks such as AGAGE or NOAA CCGG? (2) Will high-frequency isotopologue observations be valuable for constraining emissions from different sources on national scales?

[8] This study will be conducted using model-generated 'pseudo' observations. We compare two sets of emissions, calculated: (1) using pseudo mole fraction data alone, and (2) using pseudo mole fraction and isotopic composition data. While the absolute uncertainties on emissions estimated in these two types of inversion will be an underestimate of the true uncertainty that would be derived using real data, the relative reduction in uncertainty due to the addition of isotopic observations should be indicative of that which would be obtained in the real world.

1.1. Methane Isotopologues and the Next Generation of Measurements

[9] The two major isotopologues of atmospheric CH_4 differ from the most abundant form, $^{12}CH_4$, by the addition of a neutron to either the carbon atom ($^{13}CH_4$) or to one of the hydrogen atoms (CH_3D). Isotopic composition is usually quantified relative to some reference isotope ratio. These so-called 'δ-values' are defined, for the major CH_4 isotopologues, as:

$$\delta^{13}C = 1000\left(\frac{R_{^{13}CH_4}}{R_{PDB}} - 1\right) \quad (1)$$

$$\delta D = 1000\left(\frac{R_{CH_3D}}{R_{VSMOW}} - 1\right) \quad (2)$$

where R_X is the molar ratio of isotopologue X to the most abundant isotopologue. The two reference ratios are: R_{PDB}, the $^{13}C/^{12}C$ ratio found in Pee Dee Belemnite (PDB), with a value of 1123.72×10^{-5} [*Craig*, 1957] and R_{VSMOW}, the D/H ratio found in Vienna Standard Mean Ocean Water (VSMOW), with a value of 155.95×10^{-6} [*DeWit et al.*, 1980]. We will refer to the two delta values as $\delta^{13}C$ and δD throughout.

[10] Close the the earth's surface, atmospheric CH_4 currently has a mean mole fraction close to 1800 nmol mol^{-1} [e.g., *Rigby et al.*, 2008], a mean $\delta^{13}C$ of −47.1 and a mean δD of −86 [*Whiticar and Schaefer*, 2007].

[11] The next generation of CH_4 isotopologue observations will use continuous wave quantum cascade lasers [e.g., *Nelson et al.*, 2008; *Tuzson et al.*, 2008]. When combined with preconcentration techniques [e.g., *Miller et al.*, 2008; *Potter*, 2011], measurements may be possible at up to hourly frequency, with precisions potentially as high as 0.01‰ for $\delta^{13}C$ and 0.1‰ for δD [*Zahniser et al.*, 2009; S. Ono (MIT) and D. Nelson (Aerodyne), personal communication, 2011]. In this study, we test the sensitivity of our conclusions to a range of measurement repeatabilities that may eventually be achieved.

2. Methodology

[12] To perform a CH_4 isotopologue observing system simulation experiment, we rely entirely on CTM-generated 'pseudo-observations'. In this section, we first describe two possible configurations of an isotopologue network before describing the CTMs that we will use to generate output at the measurement locations. We then describe the CH_4 sources that are input to the CTMs and outline how the simulations were performed. Finally, we discuss the inversion methodology.

2.1. Measurement Networks

[13] Two potential measurement network types have been used in this work. The first type, based on the AGAGE network, makes high-frequency in situ measurements at 11 locations (see Figure 1). The advantage of this type of network is that high frequency variability can be observed, providing, for example, information about local sources. However, the cost of setting up and operating this sort of network currently limits the number of stations involved.

[14] Flask-sampling networks such as NOAA-CCGG take air samples from around the world and measure them at a central laboratory. These networks typically have a lower measurement frequency (∼weekly samples, compared to ∼hourly for in situ observations), but higher spatial coverage. Existing flask networks generally attempt to sample air during periods when local influences are small. The locations of the existing NOAA-CCGG sampling positions is shown in Figure 1.

2.2. Atmospheric Chemical Transport Models

[15] The first question that we have posed requires the use of a global chemical transport model to address, while the second, which concerns national emissions, requires sensitivity to emissions on smaller scales. Here we use a global Eulerian CTM for the first and a Lagrangian regional model for the second.

[16] Global simulations were performed using the Model for OZone and Related Tracers (MOZART v4.5) [*Emmons et al.*, 2010]. MOZART is an Eulerian CTM that calculates trace gas transport and chemistry using reanalyzed meteorological fields. The National Center for Environmental Prediction/National Center for Atmospheric Research

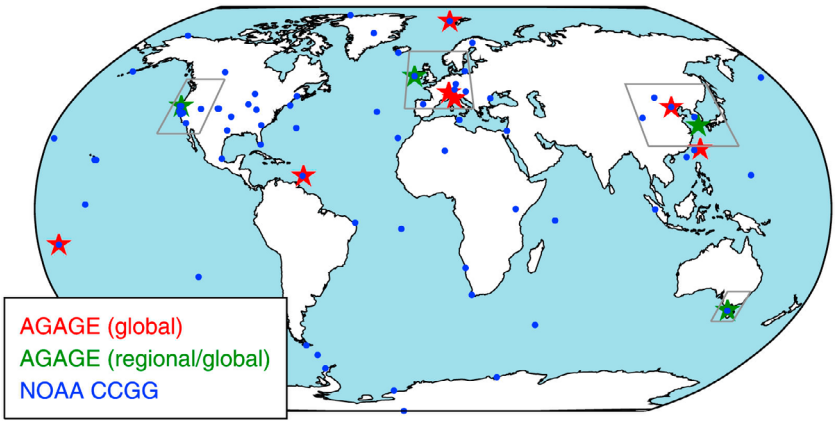

Figure 1. Location of AGAGE stations used in the global inversions (red stars), AGAGE sites used in both the global and regional inversions (green stars) and NOAA CCGG sites (blue circles). The grey boxes show the domains used in the regional inversions.

reanalysis was used for this purpose [*Kalnay et al.*, 1996], with a resolution of approximately 1.9° × 1.9° and 28 vertical levels. This model has been shown to simulate CH_4 mole fractions well at the surface [*Patra et al.*, 2011].

[17] Regional simulations were performed using the UK Met. Office Numerical Atmospheric Modeling Environment (NAME v3) [*Ryall et al.*, 1998; *Manning et al.*, 2011]. NAME is a Lagrangian particle dispersion model (LPDM), which calculates the sensitivity of each observation to emissions from grid cells surrounding a measurement site by tracking ensembles of 'particles' backwards in time. Back trajectories of 13-day duration were calculated (13 days being long enough for the majority of the particles to leave the domains of interest) using the UK Met. Office analysis fields at 0.38° × 0.56° horizontal resolution and 37 vertical levels. This model has been used extensively for long-lived trace gas emissions estimation on national scales [e.g., *Manning et al.*, 2011]. Here we determine emissions from countries around a subset of AGAGE stations; Mace Head, Ireland, Trinidad Head, California, Gosan, South Korea and Cape Grim, Tasmania (marked in green in Figure 1). These stations are coastal sites that regularly intercept emissions from the surrounding countries and have been used in previous inversions using the NAME model [e.g., *O'Doherty et al.*, 2009; *Manning et al.*, 2011; *Rigby et al.*, 2011]. The domains within which emissions were estimated are shown as grey rectangles in Figure 1.

2.3. Methane Sources and Their Isotopic Composition

[18] Throughout this paper we use the comprehensive emissions data set compiled by *Fung et al.* [1991]. Since some more recent studies differ from these estimates for some processes, we scaled the *Fung et al.* [1991] biomass burning and fossil emissions distributions to match the global emissions from *Bousquet et al.* [2006] and EDGAR v4.2 (Emission Database for Global Atmospheric Research (EDGAR), release version 4.2., 2011, http://edgar.jrc.ec.europa.eu) respectively. Since we are primarily interested in the differences between inversions that use different pseudo data sets generated from the same emissions source distribution, any inaccuracies in the chosen emissions data set should be a second-order source of error in our conclusions.

[19] The reason to expect that CH_4 isotopologue observations can provide additional information about source partitioning, compared to whole-CH_4 observations, is that different sources emit with different isotopic ratios. For example, wetlands emit CH_4 that is relatively depleted in ^{13}C, compared to CH_4 emitted in biomass burning. Therefore, CH_4 emitted from wetlands has a lower $\delta^{13}C$ than that emitted from biomass-burning. Fossil fuel and landfill sources generally emit with $\delta^{13}C$ values in between those of biomass burning and microbial sources. For δD microbial sources are also amongst the most depleted. However, fossil emissions tend to have the highest δD values, with biomass burning and landfill falling in between.

[20] Relatively detailed estimates of source δ-values have been calculated for a wide variety of CH_4 sources [e.g., *Whiticar and Schaefer*, 2007]. However, rather than making estimates of emissions from every source, some of which are very minor, and some of which have very similar δ-values to other sources, we solve for emissions from four major processes: microbial (e.g. wetlands and rice); biomass-burning; fossil-fuel; landfills (Figure 2). These groupings are based on the analysis of *Snover et al.* [2000], whose source δ-values we use to calculate emission rates of each isotopologue input to the model. These overall calculated source isotopic ratios are given in Table 1. While *Snover et al.* [2000] provide uncertainties for their source categories, we chose source uncertainties that are twice the value used in their work, to ensure that the overall uncertainty for each source category more than spans the range given for individual sources in *Whiticar and Schaefer* [2007] (Table 1). We investigate the influence on the inversion of improving these source uncertainties in the future.

[21] The fractionation of the two isotopologues due to the OH radical is also very different and could therefore provide information on the strength of this important CH_4 sink. While the reaction rate of $^{13}CH_4$ with OH is only around 0.4% higher than that of $^{12}CH_4$, the reaction rate for CH_3D is

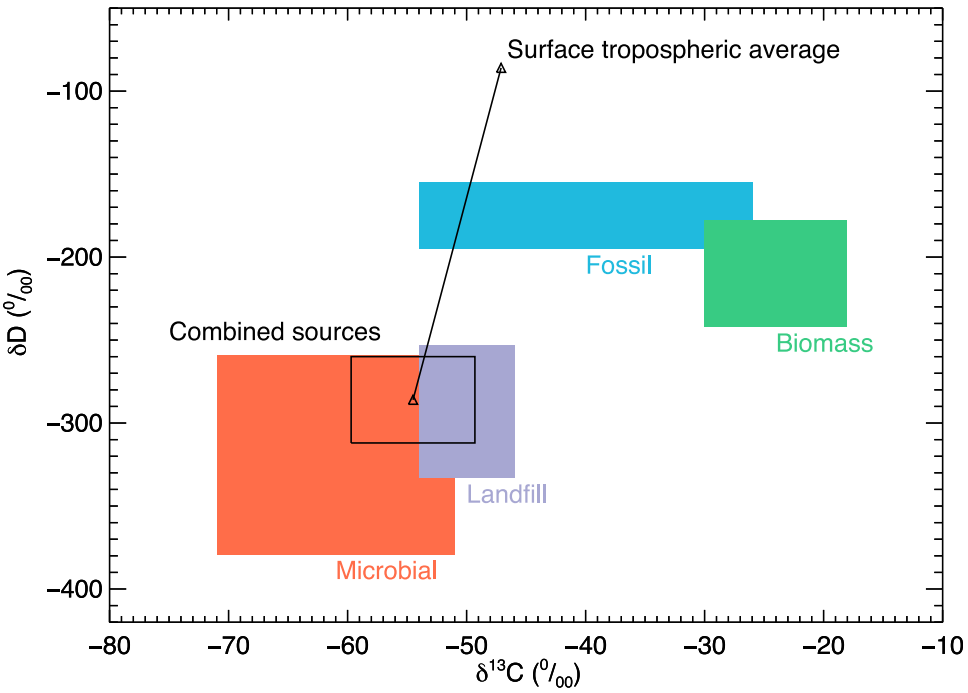

Figure 2. The $\delta^{13}C$ and δD for the four major sources whose emissions were estimated in this work. The colored areas show the 1-sigma uncertainty range used in the inversions. The triangular points show the combined source isotopic ratio and the measured ambient value. The difference between the two shows the magnitude of fractionation, primarily due to reaction with OH. Modified from *Snover et al.* [2000].

approximately 30% higher than for $^{12}CH_4$ [*Saueressig et al.*, 2001]. This leads to a measured δD in the atmosphere that around 200‰ higher than would be expected from the sum of the source isotopic ratios, compared to a fractionation of only 7.4‰ for $\delta^{13}C$ [*Whiticar and Schaefer*, 2007, Figure 2].

2.4. Modeling Atmospheric Methane Mole Fraction and Isotopic Composition

[22] Methane mole fractions were simulated in MOZART using the *Fung et al.* [1991] emissions for the year 2000, following a 5-year spin up period. At the beginning of each year of the spin-up, three-dimensional δ-value fields were adjusted, by the addition of a constant, to return the global-average surface δ-value to the observed number (see Table 1). These small adjustments were required to counter a small drift in δ-values seen in the model, due to inaccuracies in emission and fractionation rates. The mole fractions of the three isotopologues were simulated as individual tracers in the model.

[23] Emission rates of $^{13}CH_4$ and CH_3D were calculated from the *Fung et al.* [1991] emissions by multiplying emissions from each source type by the isotope ratios derived from the δ-values given in Table 1. The use of a single source isotope ratio is a significant simplification in this work. However, we investigate the influence of this simplification by determining the uncertainty in our results associated with a range of source ratios.

[24] Methane is primarily destroyed in the atmosphere through reaction with the hydroxyl radical (OH). Global monthly average three-dimensional OH concentration fields from *Spivakovsky et al.* [2000] were used in MOZART simulations. These concentrations were specified offline, meaning that the OH reacted with atmospheric CH_4, but was not itself used up in the reaction. This linear approximation can be expected to hold well for small changes in CH_4 concentration, and is routinely used in atmospheric inversions [e.g., *Chen and Prinn*, 2006; *Rigby et al.*, 2008]. Each isotopologue separately reacted with the OH field with rates

Table 1. The δ-Values and Source Strengths for the Four Aggregated Source Categories Used in This Study and the Assumed 1-σ Uncertainties in the Isotopologue Ratio[a]

Category	Sources	$\delta^{13}C$ (‰ PDB)	δD (‰ VSMOW)	Source Strength (Tg/yr)
Microbial	Wetlands, rice, ruminants, termites	−61 ± 10	−319 ± 60	311
Fossil fuel	Coal mining, gas leaks	−40 ± 14	−175 ± 20	97
Biomass burning	Biomass burning	−24 ± 6	−210 ± 32	37
Landfill	Landfill	−50 ± 4	−293 ± 40	39
Ambient Air (global average)		−47.1	−86	

[a]The Source column shows the individual source types included in each process.

recommended by *Sander et al.* [2011], based on the work of *Rust and Stevens* [1980], *Cantrell et al.* [1990], and *Gierczak et al.* [1997]. Offline reactions with stratospheric chlorine (Cl) and excited oxygen radicals (O(1D)) were parameterized, based on the model of *Velders* [1995], and overall stratospheric fractionation factors (the ratio of overall reaction rates) of 0.988 and 0.78 were applied for the $^{13}CH4$ and CH_3D isotopologues relative to CH_4 respectively [*Brenninkmeijer et al.*, 1995; *Irion et al.*, 1996]. Reactions with marine boundary layer Cl were ignored. These sinks are known to lead to additional fractionation in the atmosphere [e.g., *Platt et al.*, 2004]. However, given that they remove a relatively small quantity of CH_4 from the atmosphere and do not necessarily change along with any of the quantities investigated here, the errors induced by ignoring this factor is thought to be minimal for this study.

[25] In the regional simulations using the NAME model, it was assumed that no chemical destruction occurred. This simplification has been shown to be reasonable over the short back-trajectory timescales compared to the methane lifetime [*Manning et al.*, 2011].

2.5. Determining Emissions From Atmospheric Observations

[26] For our global simulation, we followed an approach used in many previous inversions and determined emissions from large regions at monthly resolution [e.g., *Bousquet et al.*, 2006; *Chen and Prinn*, 2006]. We used the 11 continent-sized surface regions from the TRANSCOM model inter-comparison experiment [*Gurney et al.*, 2002] and determined source strengths from the four major source categories (see above) from each region. To account for uncertainties in the initial conditions, we also solved for CH_4, $\delta^{13}C$ and δD values at the start of the simulation. These values were found in both hemispheres in the troposphere and for the stratosphere. In the results presented below, we re-aggregated the emissions from each region and each month, and present only global, annually averaged emissions uncertainties (regional uncertainty reductions are shown in the auxiliary material).[1] We note that by determining emissions from large regions and on monthly timescales, our inversions would incur so-called "aggregation errors" in a real-world inversion. These errors could lead to spurious uncertainty reductions since errors in the spatial and temporal distribution of the emissions field would not be accounted for.

[27] In the regional simulation, we determined emissions from the four source categories from countries (or parts of countries) close to four AGAGE monitoring sites (green stars in Figure 1). Again, emissions were determined on monthly timescales. We also solved for the background CH_4 mole fraction and δ-values during each month, to allow for uncertainties in the background to be propagated to our source uncertainties.

[28] Methane mole fractions and δ-values are non-linearly related to emissions, and therefore an inversion using such data will require an iterative approach to search for the optimal solution. In a Bayesian framework, such a solution is found by minimizing a so-called 'cost function', which quantifies the discrepancy both between the observations and the model, and between the solution and some prior emissions estimate [see, e.g., *Tarantola*, 2005]. In this work, we assume that the minimum of the cost function has been found (which is true in this case, since the 'data' have been generated by the model), and aim only to find the uncertainty in the solution. We make the assumption that in the region of this minimum, the relationship between the observations and parameters is linear. Therefore, the uncertainties presented are approximations of the true uncertainties.

[29] In linear inverse problems, emissions (or other parameters) can be related to atmospheric observations through a 'sensitivity matrix' (**H**) using [e.g., *Tarantola*, 2005]:

$$\mathbf{y} = \mathbf{H}\mathbf{x} + \boldsymbol{\epsilon} \tag{3}$$

The vector **y** contains the observations at various locations and times, and the vector **x** contains emissions from certain geographical regions and times, or sink strengths. The residual between the model-predicted observations and the measurements is given by the vector $\boldsymbol{\epsilon}$. The sensitivity matrix (**H**) is a matrix of partial derivatives, which can be approximated as finite differences in linear problems, such that:

$$H_{ij} = \frac{\Delta y_i}{\Delta x_j} \tag{4}$$

These finite differences can be found by running the CTM N times (where N is the number of elements in **x**), with parameters (e.g. emissions) independently perturbed by some amount in each region in each run (Δx_j). The resulting change in observable can then be extracted from the CTM output from each run at the measurement location and time.

[30] If the model-measurement uncertainties can be assumed independent, the uncertainty covariance (**R**) is a diagonal matrix, such that:

$$diag\,(\mathbf{R}) = \boldsymbol{\sigma}^2 \tag{5}$$

where σ is a vector of measurement and modeling uncertainties, in which each element is the uncertainty in the corresponding element of **y**. Here, we assume that overall uncertainties include contributions from the measurement repeatability (σ_M), model-data representation error (σ_{RE}), sampling frequency (σ_{SF}) and uncertainties in the observations induced by errors in the source isotope ratios (σ_{SIR}):

$$\boldsymbol{\sigma} = \sqrt{\boldsymbol{\sigma}_M^2 + \boldsymbol{\sigma}_{RE}^2 + \boldsymbol{\sigma}_{SF}^2 + \boldsymbol{\sigma}_{SIR}^2} \tag{6}$$

For the global simulations, the representation error was calculated as the standard deviation of the mole-fractions or δ-values in the eight grid cells surrounding each site [*Chen and Prinn*, 2006]. This information does not exist for the LPDM, so for the regional simulations the representation error was estimated as the standard deviation of the modeled mole fraction variability within each averaging period [*Rigby et al.*, 2011]. The sampling frequency error is a measure of each site's ability to capture the entire

[1] Auxiliary material data sets are available at ftp://ftp.agu.org/apend/jd/2011jd017394. Other auxiliary material files are in the HTML. doi:10.1029/2011JD017384.

variability within an averaging period. It was calculated here as the modeled variability within each averaging period, divided by the square root of the number of observations within that period.

[31] The uncertainty term related to inaccuracies in the source isotope ratios (σ^2_{SIR}), which only applies to the isotopologue measurements, was estimated by performing 50 perturbed forward runs of the CTM. In each run, the isotopologue emissions from each region were calculated from source delta values randomly selected from a Gaussian distribution with standard deviations given in Table 1. By assuming that source isotopologue ratios vary between different regions, we are assuming that the uncertainties stem from geographical differences in the source ratio, rather than an inability to quantify a globally uniform source ratio. The term σ^2_{SIR} is calculated at each model time step as the standard deviation of atmospheric delta values predicted in the 50-member ensemble.

[32] Note that the above uncertainty calculation assumes that the measurements are unbiased, and that any errors are random with a Gaussian probability density function. Any significant uncharacterized biases in the new measurements could reduce the true uncertainty reduction obtained in an inversion.

[33] In this paper, the observations vector contains either mole fractions alone or mole fractions and isotopic data. Therefore, the uncertainty vector, and the sensitivity matrix, varies in each experiment. For the mole fraction only inversion:

$$\boldsymbol{\sigma} = \boldsymbol{\sigma}_{CH_4} \tag{7}$$

$$\mathbf{H} = \mathbf{H}_{CH_4} \tag{8}$$

where σ_{CH_4} is a vector of CH_4 mole fraction total uncertainties and $\mathbf{H}_{CH_4}$ is a matrix of sensitivities of mole fractions to emissions changes.

[34] For the mole fraction and isotopologue inversions, the uncertainty vector and sensitivity matrix is made up of subvectors and sub-matrices corresponding to mole fractions and δ-values:

$$\boldsymbol{\sigma} = \left(\boldsymbol{\sigma}_{CH_4}, \boldsymbol{\sigma}_{\delta^{13}C}, \boldsymbol{\sigma}_{\delta D}\right)^T \tag{9}$$

$$\mathbf{H} = \left(\mathbf{H}_{CH_4}, \mathbf{H}_{\delta^{13}C}, \mathbf{H}_{\delta D}\right)^T \tag{10}$$

The uncertainties for each isotopologue in equation 9 are calculated individually using equation (6).

[35] In the inversions that use both mole fractions and isotopologues, we include off-diagonal elements in the model-measurement uncertainty covariance (**R**). These elements reflect the correlation between the model representation error for the three sets of observations, since the three sets of measurements are co-located. We estimate the size of these terms using the correlation between the forward-model time series at each measurement site. The covariance between uncertainties for isotopes A and B at site s and time t is given by:

$$Cov(A,B)_{s,t} = \rho_s \sigma_{re,A,s,t} \sigma_{re,B,s,t} \tag{11}$$

where ρ_s is the correlation coefficient of the two sets of observations at site s over the period of interest.

[36] Assuming that all uncertainties follow a Gaussian distribution we obtain the posterior uncertainty covariance matrix using [e.g., *Tarantola*, 2005]:

$$\mathbf{P} = \left(\mathbf{H}^T \mathbf{R}^{-1} \mathbf{H} + \mathbf{P}_{ap}^{-1}\right)^{-1} \tag{12}$$

Here $\mathbf{P}_{ap}$ is the prior uncertainty covariance matrix.

3. Forward Modeling

3.1. Global-Model Mole Fraction and Isotopologue Time Series

[37] Daily average CH_4 mole fractions and δ-values predicted by the MOZART model for the year 2000 are shown for the AGAGE site at Mace Head-on the West coast of Ireland in Figure 3. Monthly averaged mole fraction and δ-value time series' at every other model grid cell are provided in netCDF format in the auxiliary material. Figure 3 shows crosses at times when we assumed that the NOAA CCGG network took samples. The NOAA network largely attempts to avoid polluted air masses. To reflect this, we assumed that flask samples were taken on the day with the minimum mole fraction in each week.

[38] Figure 3 shows a mole fraction seasonal cycle that is similar to that seen in AGAGE observations (see auxiliary material). The seasonal changes at Mace Head are dominated by variations in the rate of destruction by OH, which tends to lead to a CH_4 minimum in the northern hemisphere summer, and the boreal wetland emission cycle, which peaks in the summer/fall. The influence of OH can be seen as a drop in mole fraction throughout the spring, while the competing influence of increased wetland emissions begins to dominate from the summer and throughout the fall. The magnitude of the wetland emission-induced increase in mole fraction during the fall is larger than found in the AGAGE observations, which likely reflects an overly strong seasonal cycle in the *Fung et al.* [1991] wetland emissions cycle.

[39] The seasonal cycle in the two isotopologues is also dominated by OH and wetland emissions variations. The increasing northern hemisphere OH concentration during the spring and summer tends to increase the δ-value of both isotopologues, with a larger increase in δD due to its larger OH fractionation. In contrast, increasing summertime northern hemisphere wetland emissions tend to reduce the δ-values of both isotopologues, since the wetland emissions are relatively depleted in each isotopologue, compared to ambient air.

[40] Overlaid on top of the seasonal cycle in background CH_4 mole fractions and δ-values are 'pollution events', with durations of days or weeks (as shown in the auxiliary material, the variability seen in these pollution events is of similar magnitude to the measured mole fractions). These occur when air is advected to Mace Head from Europe under Easterly winds. At Mace Head, these pollution events tend to lower the δ-values of both isotopologues, largely reflecting the influence of microbial European sources. Episodes of elevated δ-values of both isotopologues are seen at Mace Head when CH_4 levels decrease, potentially indicating the advection of air from lower latitudes, which tends to have a

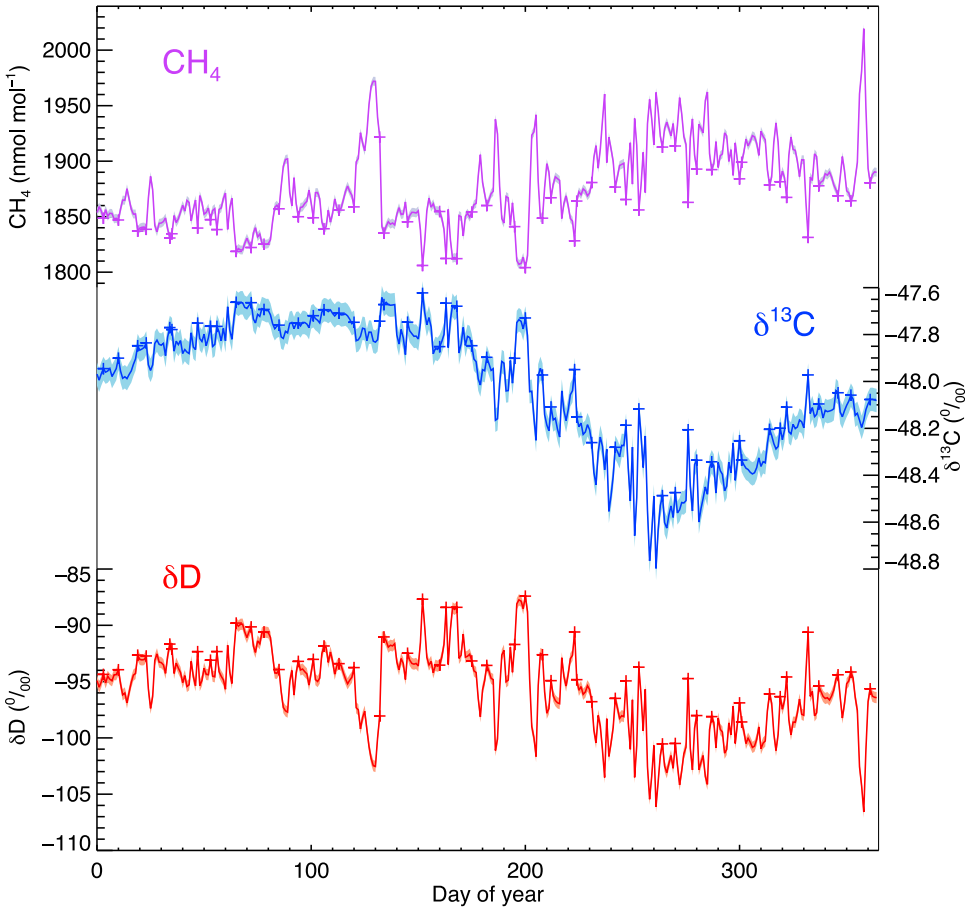

Figure 3. Model-generated daily average (top) methane mole fractions, (middle) $\delta^{13}C$ and (bottom) δD (bottom), for the year 2000 at Mace Head, Ireland. Crosses indicate times for which flask samples were collected. Shading shows the uncertainty range ±4 ppb, ±0.05‰ and ±0.5‰ on the CH4, $^{13}CH_4$ and CH_3D observations, respectively.

lower mole fraction and higher isotopologue ratio. The attribution of these features to specific processes can be more clearly seen by perturbing each source and modeling the resulting change in mole fraction or δ-value, as shown in the next subsection.

3.2. Sensitivity of Observations to Global Emissions and Sink Perturbations

[41] In order to invert for particular sources and sinks from atmospheric measurements, we need to know the how a change in these quantities influences the observations. Such sensitivities can be estimated using an atmospheric chemical transport model.

[42] To determine the sensitivity of Mace Head CH_4 measurements to changes in emissions from each region and each of the four source categories shown in Table 1, and to a change in the OH concentration, we increased each quantity by 10% compared to the reference run presented above, and tracked the resulting change in CH_4, $^{13}CH_4$ and CH_3D mole fraction in the model. We calculated the δ-values of these "perturbed" runs and subtracted the reference mole fractions and δ values shown in the previous subsection. The resulting "sensitivities" to source and sink changes, summed over the whole globe for an entire year and divided by the size of the perturbation in Tg, are shown in Figure 4.

[43] Figure 4 shows that an increase in emissions from each source type leads to an increase in mole fraction throughout the course of the one-year investigation period, while an increase in OH concentration leads to a decrease in CH_4 mole fraction at Mace Head. Similar "per kilogram" increases in mole fraction are seen for microbial, fossil and landfill emissions. The smaller overall response of biomass burning emissions reflects the larger distance of these sources from the site. Changes in mole fraction due to an OH change can be seen to accelerate at Mace Head during the summer, when northern hemispheric OH concentrations are highest. The increase in mole fraction due to an increase in microbial sources peaks in the late summer/fall due to increased boreal wetland emissions during this season. In contrast, changes in mole fraction due to fossil and landfill sources are seen to increase steadily throughout the year, reflecting the assumption that these sources do not have a seasonal cycle in the *Fung et al.* [1991] estimates. Each of these sensitivities shows short timescale fluctuations (days–weeks) at Mace Head, indicating synoptic-scale changes in the source-receptor relationship.

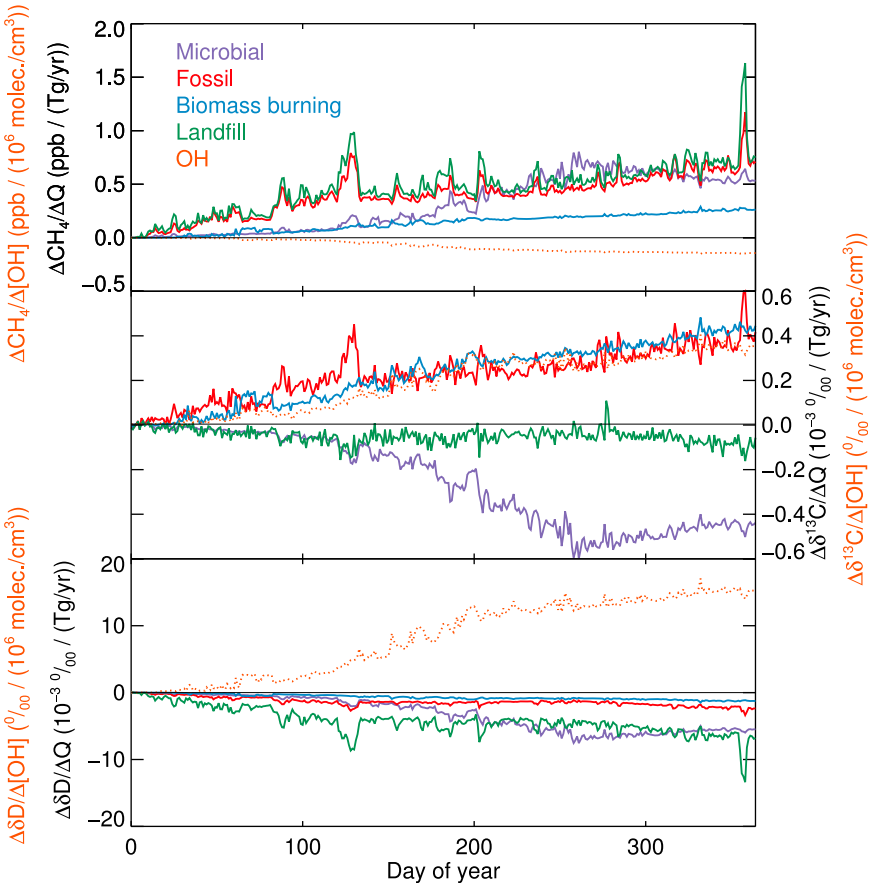

Figure 4. Global, annual-total sensitivities of daily average (top) methane mole fractions, (middle) $\delta^{13}C$ and (bottom) δD, to a unit increase in global source strength or OH concentration for the year 2000 at Mace Head, Ireland.

[44] Changes in δ-values at Mace Head cannot simply be interpreted by considering whether a change in some parameter tends to either increase or decrease the atmospheric burden, as with mole fractions. Rather, the strength and isotopic signature of the source relative to background air must be considered. Reflecting this, Figure 4 shows that an increase in the global microbial source tends to reduce the δ-value of both isotopologues since microbial sources are relatively depleted in both, compared the background atmosphere. As with the mole fraction, changes due to microbial sources peak in the late summer/fall when wetland emissions are largest.

[45] A biomass burning increase induces a larger change in $\delta^{13}C$ than might be expected from the moderate mole fraction change noted above. This is because its $\delta^{13}C$ is very much higher than the background atmosphere. In contrast, landfills have very little influence on $\delta^{13}C$ at Mace Head, because their isotope ratio is very similar to that of ambient air. For similar reasons, biomass burning and fossil sources have a smaller influence on δD than landfills, which have an isotope ratio that is the further away from atmospheric δD.

[46] An increase in OH concentration tends to increase the δ-value of both isotopologues. However, this change is larger for δD than for $\delta^{13}C$, since the fractionation due to OH is larger for CH_3D than for $^{13}CH_4$. Based on the higher sensitivity δD observations to OH changes, we would expect that δD observations should provide a stronger constraint on global OH levels than $\delta^{13}C$, given a similar relative uncertainty on the observations.

4. Uncertainty Reduction due to New Isotopologue Observations

4.1. Reduction in Global Source Uncertainty

[47] We performed two sets of inversions to determine global uncertainty reduction: one using pseudo data at 11 high-frequency AGAGE stations, and one using low frequency pseudo flask samples at 73 NOAA CCGG sites (Figure 1). The sensitivities of these observations to changes in emissions each month, from each of the four source categories from 11 TransCom regions was calculated [*Gurney et al.*, 2002]. The global OH concentration was also solved for in each month, along with initial mole fractions and δ values (from two tropospheric and one stratospheric regions), resulting in 549 elements in the parameters vector ($\mathbf{x}$) in each inversion. The initial uncertainty on each source from each region was assumed to be 100% of the prior estimates, as used in previous inversions [*Chen and Prinn*, 2006]. The prior uncertainty on the OH concentrations and initial conditions was also assumed to be 100%.

[48] In the high-frequency inversions, daily averaged pseudo-observations were used, whereas in the low-frequency

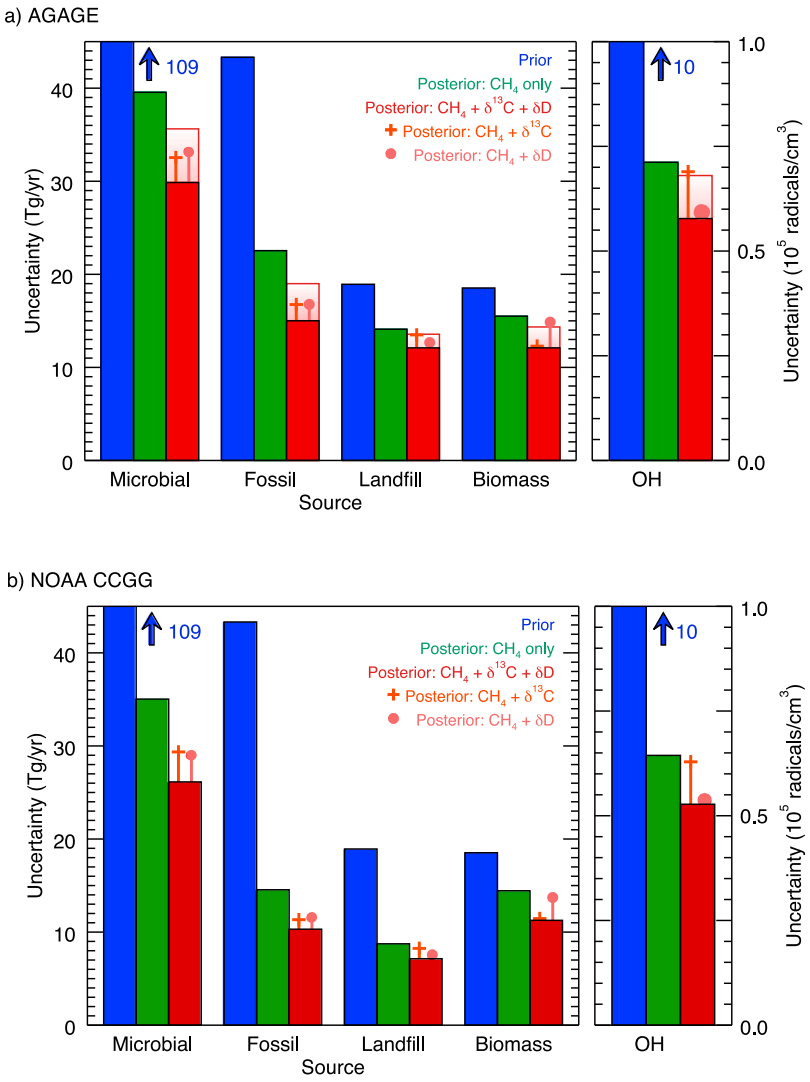

Figure 5. Uncertainties on global sources or OH sink before each inversion (blue bars) and following inversions using mole fractions only (green bars) or mole fractions, $\delta^{13}C$ and δD observations (red bars), for (a) the AGAGE network and (b) the NOAA CCGG network. Single lines with a cross on top show the posterior uncertainty for inversions using mole fractions and $\delta^{13}C$ only, and single lines with a circle on top show the posterior uncertainty for inversions using mole fractions and δD only. The shaded red bars in the background of Figure 5a show the a posteriori uncertainty when low-frequency (weekly) isotopologue observations were included in an inversion also using daily AGAGE CH_4 observations. Measurement repeatibilities of ± 4 ppb, ± 0.05‰ and ± 0.5‰ were used for the CH4, $^{13}CH_4$ and CH_3D observations respectively.

inversion, one observation was used per week. The overall uncertainty included measurement uncertainty, representation error, sampling frequency error and source emissions uncertainty (equation (6)). We assumed that the measurement uncertainty was equal to the repeatability, which was estimated as 4 ppb for CH_4 [*Chen and Prinn*, 2006] and 0.05‰ for $\delta^{13}C$ and 0.5‰ for δD. These δ-value uncertainties represent the higher end of the anticipated range but are thought to be an achievable target. The influence of a change in these isotopologue precisions, and in the source uncertainty, is investigated in the next subsection. In the inversions discussed below, only global-total posterior uncertainties are shown, rather than monthly, regional averages (regional uncertainty reductions are shown in the auxiliary material).

[49] For both networks, the first test we performed was to estimate the level of uncertainty reduction obtained when one year of daily CH_4 mole fraction measurements were used. Figure 5 shows the global-total prior uncertainty for each source and the OH concentration in blue, and the posterior uncertainty for this CH_4-only inversion in green. Figure 5a shows the uncertainties for the high-frequency (AGAGE) network, while Figure 5b shows the uncertainties for the flask (NOAA CCGG) network. Uncertainty reductions of at least 15% are seen for all annual-mean global sources in this inversion, with similar uncertainty reductions for both networks.

[50] Next, we determined the posterior uncertainty for inversions using CH_4 mole fractions and $\delta^{13}C$ and δD (red

Table 2. Relative Annual-Mean Uncertainty Reduction, Compared to the Mole-Fraction Only Inversion, for Each Network and for Each Global Source/Sink[a]

	High-Frequency Network (AGAGE)	Flask Network (NOAA CCGG)
Microbial (Tg/yr)	−9.7 (3%)	−8.9 (3%)
Fossil (Tg/yr)	−7.5 (8%)	−4.2 (4%)
Biomass (Tg/yr)	−3.4 (9%)	−3.2 (9%)
Landfill (Tg/yr)	−2.0 (5%)	−1.6 (4%)
OH (10^5 radicals/cm^3)	−0.13 (1%)	−0.12 (1%)

[a]Using repeatabilities of ±4 ppb, ±0.05‰ and ±0.5‰ on the CH_4, $^{13}CH_4$ and CH_3D observations respectively. The numbers in brackets show the uncertainty reduction as a percentage of the total source or sink.

bars). In every case, substantial further error reduction was obtained, compared to the mole fraction-only inversion (see also Table 2). In absolute terms, the largest uncertainty reductions were for microbial sources, although this represents a relatively small fraction of the total source (~3%). The largest fractional uncertainty reductions were for biomass burning (9%) and fossil sources (8% and 4% for the high frequency and flask networks respectively). Small reductions in a posteriori correlations between the global sources was also seen when the new measurements were included in the inversion (see auxiliary material).

[51] Two further inversions were performed for each network, using CH_4 mole fractions and one of the two sets of δ-values. This allowed us to quantify the influence of each isotopologue measurement on the inversion. The relative uncertainty reduction due to each isotopologue observation is determined by its uncertainty and the sensitivity to changes in emissions. As discussed in section 3.2, the latter is a function of the source strength and the source isotope ratio relative to ambient air. Following on from the conclusions drawn in section 3.2, we note some of the more prominent signals, namely that: uncertainty reduction for biomass burning emissions are dominated by the $\delta^{13}C$ measurement, reflecting its very high δ-value relative to air; for similar reasons, the additional uncertainty reduction for landfills is dominated by δD; there is a larger uncertainty reduction on the OH concentration due to δD than $\delta^{13}C$, reflecting the larger fractionation of this isotopologue due to OH.

[52] Finally, to investigate the role that measurement frequency played in the uncertainty reduction, we performed one further inversion with the high-frequency network, in which the isotopologue measurements were made at the

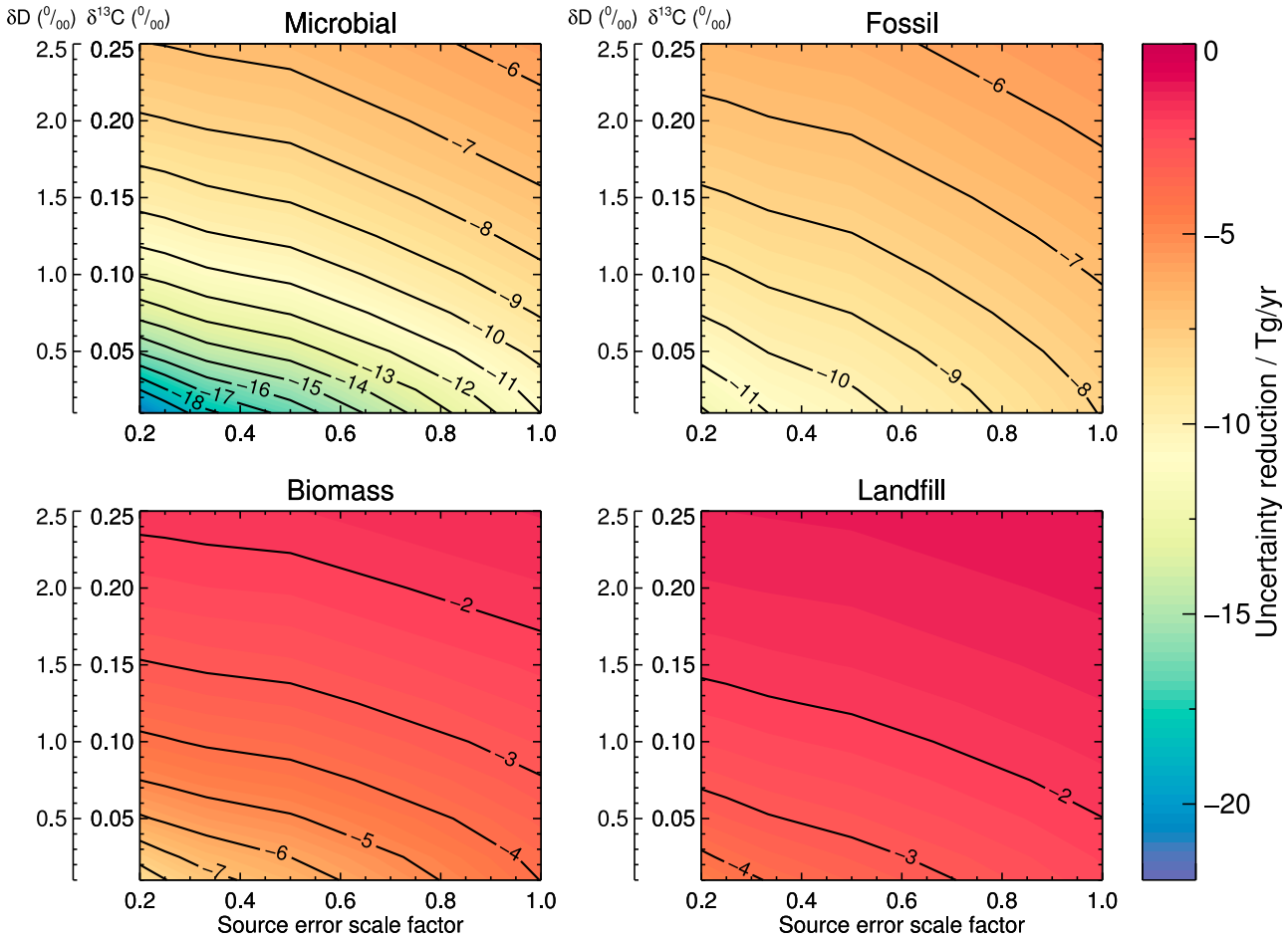

Figure 6. Uncertainty reduction, compared to a mole-fraction only inversions, for a range of δ-value precisions and source isotopic ratio uncertainty scaling factors for the AGAGE network. The source isotopic ratio uncertainty scaling factors multiply the uncertainties shown in Table 1. Both uncertainties are used in the inversion as shown in equation (6).

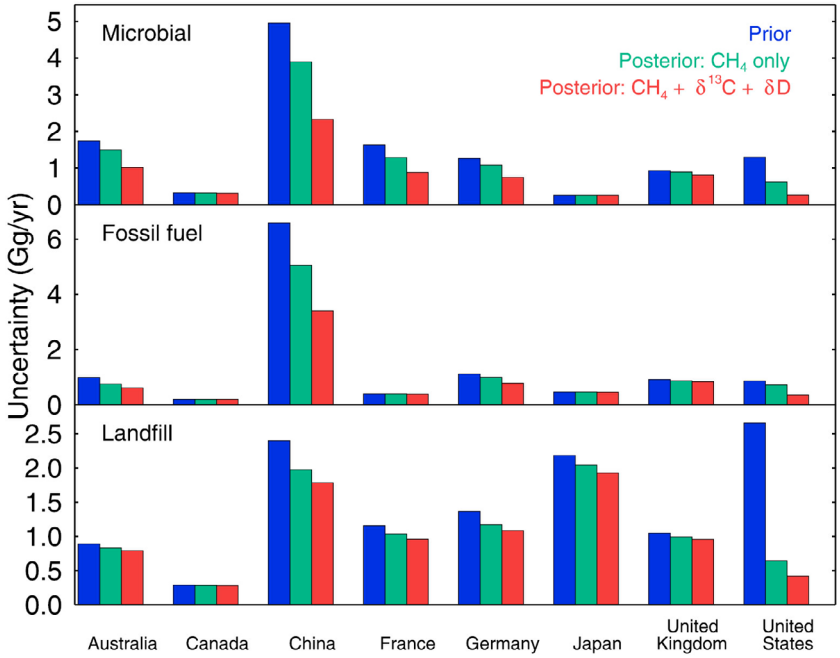

Figure 7. Uncertainties on sources in countries close to the AGAGE sites. The blue bars show the prior uncertainty, the green bars show the posterior uncertainty following a mole fraction-only inversion and the red bars show the posterior uncertainty following a mole fraction and isotopologue inversion. Note that only parts of some countries lie within the inversion domains.

same times as the flask network (once per week). The results of this inversion (red shaded bars in the background of Figure 5a) show that the a posteriori uncertainty is significantly larger for the CH_4 + isotopologue inversion when a lower isotopic measurement frequency is used. Smaller uncertainty reductions (e.g. 4 Tg/yr compared to 9 Tg/yr for the microbial source) are also obtained, compared to the CH_4-only inversion.

4.2. The Influence of Measurement and Source δ-Value Uncertainties

[53] We performed several inversions using the method outlined above in which the anticipated δ-value repeatability was varied, or the source δ-value uncertainty was reduced by a scaling factor. We assumed that the repeatability scaled proportionally for both isotopologues, reflecting an assumption that improvements in measurement techniques will equally impact the precision of both measurements. Likewise, we applied the same scaling factor to the source δ values for each of the source categories.

[54] The difference between the mole fraction-only and mole fraction-plus-isotopologue posterior uncertainties is shown in Figure 6. Figure 6 shows that the uncertainty reduction is sensitive to changes in the measurement precision, with improvements of 10 Tg/yr over the range of precisions investigated here for microbial sources. Reductions in the uncertainty of the source isotopologue ratios were found to lead to more modest uncertainty reductions in the inversion. The influence of improved source uncertainty reduction increases as measurement precision increases, perhaps indicating a small "saturation" in the information that can be derived from improvements in measurement technology alone.

4.3. Uncertainty Reduction on National Scales

[55] To investigate whether CH_4 isotopologue information could provide additional uncertainty reduction on national scales (e.g. for emissions verification), we used a regional Lagrangian particle dispersion model to calculate sensitivity functions in limited domains around four AGAGE sites (see Figure 1). The NAME model (see section 2.2) directly calculates the sensitivity of each measurement to changes in emissions from each of the surrounding grid cells. These sensitivities were aggregated into national totals, and emissions uncertainties from the largest national emitters close to the AGAGE sites were evaluated. Emissions from three source types were estimated for each country: microbial, fossil and landfill. Biomass burning was not investigated, because significant pollution events due to biomass burning were not regularly found at these sites (using the *Fung et al.* [1991] source distribution). Note that only parts of some countries (e.g. USA) are covered by the regional domains.

[56] Inversions were performed assuming 100% prior uncertainty on each source within each country, and using daily average observations. Similarly to the previous section, two inversions were performed: one using mole fraction observations only (green bars in Figure 7) and one using mole fractions, $\delta^{13}C$ and δD (red bars).

[57] The level of uncertainty reduction varies significantly depending on the sensitivity of the network to emissions from a particular country and to the size of each source within the country. For example, little uncertainty reduction is found following either inversion for microbial and fossil emissions in Japan, due to the small source strength predicted by *Fung et al.* [1991] for this country. However, larger uncertainty reduction is seen for landfill which the inventory predicts to be a large source in Japan. Depending

on the country and source, further uncertainty reductions of between 0% and 43% of the total national source strength are found by including the new observations in the inversion. The average additional uncertainty reduction due to the isotopologue observations is 13% for the domains used here. The largest total uncertainty reductions are found for emissions from the USA and China (although note that large parts of both countries are not included in the inversion domain). This suggests that emissions from these two major emitters could be further constrained by including isotopologue observations in the AGAGE network.

5. Discussion and Conclusions

[58] New developments in quantum cascade laser spectroscopy, along with sample preconcentration techniques, are predicted to lead to a new generation of high-frequency and precision measurements of the two major isotopologues of atmospheric CH_4 ($^{13}CH_4$ and CH_3D.) The purpose of this work is to determine the extent to which the high-frequency variability in atmospheric δ-values should be resolvable by these new systems, and critically examine their utility for CH_4 source and sink inversions.

[59] Using a global chemical transport model and the *Fung et al.* [1991] emissions inventory, we predicted δ-values across the globe, and have shown one year of daily average mole fractions and δ values at Mace Head, Ireland (Figure 3). At this site (and all others) it was found that the predicted precision of the new measurements should be small enough to resolve the seasonal cycle, and, for the first time, most of the short-timescale (daily weekly) variability due to the interception of 'pollution events'.

[60] We then investigated the influence of a change in emissions from each of four source types or in the OH concentration on the new measurements. The four source types were microbial sources, fossil fuel manufacturing and use, landfills and biomass burning, following the categorization by *Snover et al.* [2000]. Using these calculated sensitivities, we find that over the course of one year, changes in $\delta^{13}C$ and δD due to (for example) a change in global microbial emissions of the order of a few percent should be detectable at the anticipated precision of the instruments. Similarly, changes OH concentrations of a few percent should lead to a detectable change in δD.

[61] We investigated to what extent these sensitivities could be used to improve global inversions if networks such as AGAGE or NOAA CCGG implemented the new technology. Following a Bayesian approach using 'pseudo data', we determined uncertainty reductions, compared to a 100% assumed prior uncertainty on each source from 11 TRANSCOM regions. Inversions were carried out using mole fraction-only and then mole fraction and isotopologue data. Compared to the mole fraction-only inversion using the high-frequency network, uncertainty reductions of 10, 8, 3 and 2 Tg/yr were obtained for microbial, fossil, biomass burning and landfill sources respectively in the isotopologue inversion, using the AGAGE network.

[62] Measurements of each isotopologue were found to contribute similarly to the overall uncertainty reduction, apart from for biomass burning, where the uncertainty reduction was dominated by $\delta^{13}C$, and landfill and OH estimates where δD was more important. The relative uncertainty reduction in the source strength due to each isotopologue depended primarily on the separation between the δ-value of ambient air and the source δ-value. For the OH estimates, δD contributed more strongly due to the larger fractionation of the CH_3D isotopologue than $^{13}CH_4$.

[63] When compared to the global total emission rate for each source type, these uncertainty reductions are relatively small (3–9%). However, when compared to uncertainties calculated in previous inversions, they show that isotopologue observations could lead to meaningful further uncertainty reductions. For example, *Chen and Prinn* [2006] calculate uncertainties of approximately 40 Tg/yr on the two major microbial sources (wetlands and rice). Our calculations indicate that these uncertainties could be further reduced by around 20–30% through the addition of isotopologue observations. The magnitude of these uncertainty reductions is consistent with previous inversions that have used isotopic information. For example *Mikaloff-Fletcher* [2004a] found additional uncertainty reductions of a few Tg/yr on global CH_4 sources using a more limited flask network of $\delta^{13}C$ observations than that proposed here.

[64] We investigated whether these observations could be used to more tightly constrain national emissions of each source. Similar to the global inversion, we find that isotopologue measurements contained information on national CH_4 sources that is not present in the mole fraction data. Average uncertainty reductions of the order of 10% of the national source strengths were found, with a large degree of variation depending on the sensitivity of the network to particular countries, and the magnitude of each source within each country.

[65] The major limitation of the method used in this paper is that errors associated with chemical transport model biases have not been included. The derived posterior uncertainties are very likely to be too small, and we are therefore limited to discussing comparative reductions in uncertainty in different idealized inversions. To investigate the influence of chemical transport model uncertainty on a CH_4 isotopologue inversion, one possible approach would be to use multiple chemical transport models [e.g., *Gurney et al.*, 2002]. We also note that our inverse method assumes that the uncertainties of the new measurements are well characterized and unbiased. Any significant biases in the new instruments, or in calibration scale propagation (for example) could significantly reduce the uncertainty reduction obtained in the real world. A further limitation of this work is that only two possible network configurations have been investigated, based on existing observations. It is possible that a future monitoring system will have a significantly different configuration and that different uncertainty reductions could result. However, we note that in the two very different setups used here, very similar posterior uncertainty changes were found, suggesting that our conclusions may be more widely applicable.

[66] In summary, we have shown that new measurements of the two main isotopologues of atmospheric CH_4 ($^{13}CH_4$ and CH_3D) should provide improved constraints on global CH_4 sources and sinks. Similar levels of uncertainty reduction reduction (of the order of a few Tg/yr, or 3–9% of the overall source strengths) were found for global sources when either a flask or in-situ network were instrumented, with

similar contributions from measurements of both isotopologues. Since only one instrument would need to be purchased to provide global coverage for a flask network, there may be cost a cost advantage to instrumenting a network like NOAA CCGG, compared to AGAGE. However, we note that high frequency in situ observations from a network such as AGAGE would also allow emissions at national scales to be further constrained, potentially reducing uncertainties by a few tens of percent in countries close to the monitoring sites.

[67] **Acknowledgments.** Matthew Rigby and Ron Prinn were supported, through the AGAGE research program, by the NASA Upper Atmospheric Research Program in the U.S. with grants NNX07AE89G and NNX11AF17G to MIT. Matthew Rigby is also funded by Advanced Fellowship NE/I021365/1 from the UK Natural Environment Research Council (NERC). We are very grateful to Shuhei Ono and Kat Potter at MIT and David Nelson and Mark Zahniser at Aerodyne Research Incorporated for their work on optical isotopologue measurements and sample preconcentration that prompted this investigation.

References

Allan, W., M. R. Manning, K. R. Lassey, D. C. Lowe, and A. J. Gomez (2001), Modeling the variation of $\delta^{13}C$ in atmospheric methane: Phase ellipses and the kinetic isotope effect, *Global Biogeochem. Cycles*, *15*(2), 467–481.

Bergamaschi, P., M. Braunlich, T. Marik, and C. A. M. Brenninkmeijer (2000), Measurements of the carbon and hydrogen isotopes of atmospheric methane at Izana, Tenerife: Seasonal cycles and synoptic-scale variations, *J. Geophys. Res.*, *105*(D11), 14,531–14,546.

Bergamaschi, P., et al. (2009), Inverse modeling of global and regional CH_4 emissions using SCIAMACHY satellite retrievals, *J. Geophys. Res.*, *114*, D22301, doi:10.1029/2009JD012287.

Bousquet, P., et al. (2006), Contribution of anthropogenic and natural sources to atmospheric methane variability, *Nature*, *443*, 439–443.

Brenninkmeijer, C. A. M., D. C. Lowe, M. R. Manning, R. J. Sparks, and P. F. J. van Velthoven (1995), The ^{13}C, ^{14}C, and ^{18}O isotopic composition of CO, CH_4, and CO_2 in the higher southern latitudes lower stratosphere, *J. Geophys. Res.*, *100*(D12), 26,163–26,172.

Cantrell, C. A., R. E. Shetter, A. H. Mcdaniel, J. G. Calvert, J. A. Davidson, D. C. Lowe, S. C. Tyler, R. J. Cicerone, and J. P. Greenberg (1990), Carbon kinetic isotope effect in the oxidation of methane by the hydroxyl radical, *J. Geophys. Res.*, *95*(D13), 22,455–22,462.

Chen, Y.-H., and R. G. Prinn (2006), Estimation of atmospheric methane emissions between 1996 and 2001 using a three-dimensional global chemical transport model, *J. Geophys. Res.*, *111*, D10307, doi:10.1029/2005JD006058.

Craig, H. (1957), Isotopic standards for carbon and oxygen and correction factors for mass-spectrometric analysis of carbon dioxide, *Geochim. Cosmochim. Acta*, *12*(1-2), 133–149, doi:10.1016/0016-7037(57)90024-8.

DeWit, J. C., C. M. Straaten, and W. G. Mook (1980), Determination of the absolute hydrogen isotopic ratio of V-SMOW and SLAP, *Geostand. Newsl.*, *4*(1), 33–36.

Dlugokencky, E. J., et al. (2009), Observational constraints on recent increases in the atmospheric CH_4 burden, *Geophys. Res. Lett.*, *36*, L18803, doi:10.1029/2009GL039780.

Emmons, L. K., et al. (2010), Description and evaluation of the Model for Ozone and Related chemical Tracers, version 4 (MOZART-4), *Geosci. Model Dev.*, *3*, 43–67.

Frankenberg, C., P. Bergamaschi, S. Houweling, J. F. Meirink, J. Notholt, A. K. Petersen, H. Schrijver, T. Warneke, and I. Aben (2008), Tropical methane emissions: A revised view from SCIAMACHY onboard ENVISAT, *Geophys. Res. Lett.*, *35*, L15811, doi:10.1029/2008GL034300.

Fung, I., J. John, J. Lerner, E. Matthews, M. Prather, L. P. Steele, and P. J. Fraser (1991), Three-dimensional model synthesis of the global methane cycle, *J. Geophys. Res.*, *96*(D7), 13,033–13,065.

Gierczak, T., R. K. Talukdar, S. C. Herndon, G. L. Vaghjiani, and A. R. Ravishankara (1997), Rate coefficients for the reactions of hydroxyl radicals with methane and deuterated methanes, *J. Phys. Chem. A*, *101*(17), 3125–3134.

Gurney, K. R., et al. (2002), Towards robust regional estimates of CO_2 sources and sinks using atmospheric transport models, *Nature*, *415*, 626–630.

Hein, R., P. J. Crutzen, and M. Heimann (1997), An inverse modeling approach to investigate the global atmospheric methane cycle, *Global Biogeochem. Cycles*, *11*(1), 43–76.

Irion, F. W., et al. (1996), Stratospheric observations of CH_3D and HDO from ATMOS infrared solar spectra: Enrichments of deuterium in methane and implications for HD, *Geophys. Res. Lett.*, *23*(17), 2381–2384.

Kalnay, E., et al. (1996), The NCEP/NCAR 40-Year Reanalysis Project, *Bull. Am. Meteorol. Soc.*, *77*(3), 437–471.

Lowe, D. C., M. R. Manning, G. W. Brailsford, and A. M. Bromley (1997), The 1991–1992 atmospheric methane anomaly: Southern Hemisphere ^{13}C decrease and growth rate fluctuations, *Geophys. Res. Lett.*, *24*(8), 857–860.

Lowe, D. C., et al. (1999), Shipboard determinations of the distribution of ^{13}C in atmospheric methane in the Pacific, *J. Geophys. Res.*, *104*(D21), 26,125–26,135.

Manning, A. J., S. O'Doherty, A. R. Jones, P. G. Simmonds, and R. G. Derwent (2011), Estimating UK methane and nitrous oxide emissions from 1990 to 2007 using an inversion modeling approach, *J. Geophys. Res.*, *116*, D02305, doi:10.1029/2010JD014763.

Mikaloff-Fletcher, S. E. (2004a), CH_4 sources estimated from atmospheric observations of CH_4 and its $^{13}C/^{12}C$ isotopic ratios: 1. Inverse modeling of source processes, *Global Biogeochem. Cycles*, *18*, GB4005, doi:10.1029/2004GB002224.

Mikaloff-Fletcher, S. E. (2004b), CH_4 sources estimated from atmospheric observations of CH_4 and its $^{13}C/^{12}C$ isotopic ratios: 2. Inverse modeling of CH_4 fluxes from geographical regions, *Global Biogeochem. Cycles*, *18*, GB4005, doi:10.1029/2004GB002224.

Miller, B. R., R. F. Weiss, P. K. Salameh, T. Tanhua, B. R. Greally, J. Muhle, and P. G. Simmonds (2008), Medusa: A sample preconcentration and GC/MS detector system for in situ measurements of atmospheric trace halocarbons, hydrocarbons, and sulfur compounds, *Anal. Chem.*, *80*(5), 1536–1545.

Miller, J. B., K. A. Mack, R. Dissly, J. W. C. White, E. J. Dlugokencky, and P. P. Tans (2002), Development of analytical methods and measurements of $^{13}C/^{12}C$ in atmospheric CH_4 from the NOAA Climate Monitoring and Diagnostics Laboratory Global Air Sampling Network, *J. Geophys. Res.*, *107*(D13), 4178, doi:10.1029/2001JD000630.

Monteil, G., S. Houweling, E. J. Dlugockenky, G. Maenhout, B. H. Vaughn, J. W. C. White, and T. Rockmann (2011), Interpreting methane variations in the past two decades using measurements of CH4 mixing ratio and isotopic composition, *Atmos. Chem. Phys. Discuss.*, *11*(2), 6771–6803.

Nelson, D. D., J. B. McManus, S. C. Herndon, M. S. Zahniser, B. Tuzson, and L. Emmenegger (2008), New method for isotopic ratio measurements of atmospheric carbon dioxide using a 4.3 μm pulsed quantum cascade laser, *Appl. Phys. B*, *90*(2), 301–309.

O'Doherty, S., et al. (2009), Global and regional emissions of HFC-125 ($CHF2CF_3$) from in situ and air archive atmospheric observations at AGAGE and SOGE observatories, *J. Geophys. Res.*, *114*, D23304, doi:10.1029/2009JD012184.

Patra, P. K., et al. (2011), TransCom model simulations of CH_4 and related species: linking transport, surface flux and chemical loss with CH_4 variability in the troposphere and lower stratosphere, *Atmos. Chem. Phys.*, *11*(24), 12,813–12,837.

Platt, U., W. Allan, and D. Lowe (2004), Hemispheric average Cl atom concentration from $^{13}C/^{12}C$ ratios in atmospheric methane, *Atmos. Chem. Phys.*, *4*, 2393–2399.

Potter, K. (2011), Nitrous oxide (N_2O) isotopic composition in the troposphere: Instrumentation, observations at Mace Head, Ireland, and regional modeling, PhD thesis, Mass. Inst. of Technol., Cambridge.

Prinn, R. G., et al. (2000), A history of chemically and radiatively important gases in air deduced from ALE/GAGE/AGAGE, *J. Geophys. Res.*, *105*(D14), 17,751–17,792.

Rigby, M., et al. (2008), Renewed growth of atmospheric methane, *Geophys. Res. Lett.*, *35*, L22805, doi:10.1029/2008GL036037.

Rigby, M., A. J. Manning, and R. G. Prinn (2011), Inversion of long-lived trace gas emissions using combined Eulerian and Lagrangian chemical transport models, *Atmos. Chem. Phys.*, *11*(18), 9887–9898.

Rust, F., and C. M. Stevens (1980), Carbon kinetic isotope effect in the oxidation of methane by hydroxyl, *Int. J. Chem. Kinet.*, *12*(6), 371–377.

Ryall, D. B., R. H. Maryon, R. G. Derwent, and P. G. Simmonds (1998), Modelling long-range transport of CFCs to Mace Head, Ireland, *Q. J. R. Meteorol. Soc.*, *124*(546), 417–446.

Sander, S. P., et al. (2011), Chemical kinetics and photochemical data for use in atmospheric studies: Evaluation Number 17, *Tech. Rep. 17*, Jet Propul. Lab., Pasadena, Calif.

Saueressig, G., J. N. Crowley, P. Bergamaschi, C. A. M. Brenninkmeijer, and H. Fischer (2001), Carbon 13 and D kinetic isotope effects in the reactions of CH_4 with $O(^1)$ and OH: New Laboratory measurements and

their implications for the isotopic composition of stratospheric methane, *J. Geophys. Res.*, *106*(D19), 23,127–23,138.

Snover, A. K., P. D. Quay, and W. M. Hao (2000), The D/H content of methane emitted from biomass burning, *Global Biogeochem. Cycles*, *14*(1), 11–24.

Spivakovsky, C. M., et al. (2000), Three-dimensional climatological distribution of tropospheric OH: Update and evaluation, *J. Geophys. Res.*, *105*(D7), 8931–8980.

Tarantola, A. (2005), *Inverse Problem Theory*, Soc. for Ind. and Appl. Math., Philadelphia, Pa.

Tuzson, B., J. Mohn, M. J. Zeeman, R. A. Werner, W. Eugster, M. S. Zahniser, D. D. Nelson, J. B. McManus, and L. Emmenegger (2008), High precision and continuous field measurements of $\delta^{13}C$ and $\delta^{18}O$ in carbon dioxide with a cryogen-free QCLAS, *Appl. Phys. B*, *92*(3), 451–458.

Tyler, S. C., A. L. Rice, and H. O. Ajie (2007), Stable isotope ratios in atmospheric CH_4: Implications for seasonal sources and sinks, *J. Geophys. Res.*, *112*, D03303, doi:10.1029/2006JD007231.

Velders, G. J. M. (1995), Description of the RIVM 2-dimensional stratosphere model, *RIVM Rep. 722201002*, Bilthoven, Netherlands.

Whiticar, M., and H. Schaefer (2007), Constraining past global tropospheric methane budgets with carbon and hydrogen isotope ratios in ice, *Philos. Trans. R. Soc. A*, *365*, 1793–1828.

Zahniser, M. S., et al. (2009), Infrared QC laser applications to field measurements of atmospheric trace gas sources and sinks in environmental research: Enhanced capabilities using continuous wave QCLs, *Proc. SPIE Int. Soc. Opt. Eng.*, *2*(2), 72220H, doi:10.1117/12.815172.